

Characterisation of the *Toxoplasma gondii* tyrosine transporter and its phosphorylation by the calcium-dependent protein kinase 3

Bethan A. Wallbank,¹ Caia S. Dominicus,¹
Malgorzata Broncel,¹ Nathalie Legrave,²
James I. MacRae,² Henry M. Staines³ and
Moritz Treeck ^{1*}

¹ Signalling in Apicomplexan Parasites Laboratory, The Francis Crick Institute, London, UK.

² Metabolomics Science Technology Platform, The Francis Crick Institute, London, UK.

³ Institute of Infection and Immunity, St George's, University of London, London, UK.

Summary

Toxoplasma gondii parasites rapidly exit their host cell when exposed to calcium ionophores. Calcium-dependent protein kinase 3 (*TgCDPK3*) was previously identified as a key mediator in this process, as *TgCDPK3* knockout ($\Delta cdpk3$) parasites fail to egress in a timely manner. Phosphoproteomic analysis comparing WT with $\Delta cdpk3$ parasites revealed changes in the *TgCDPK3*-dependent phosphoproteome that included proteins important for regulating motility, but also metabolic enzymes, indicating that *TgCDPK3* controls processes beyond egress. Here we have investigated a predicted direct target of *TgCDPK3*, *ApiAT5-3*, a putative transporter of the major facilitator superfamily, and show that it is rapidly phosphorylated at serine 56 after induction of calcium signalling. Conditional knockout of *apiAT5-3* results in transcriptional upregulation of most ribosomal subunits, but no alternative transporters, and subsequent parasite death. Mutating the S56 to a non-phosphorylatable alanine leads to a fitness cost, suggesting that phosphorylation of this residue is beneficial, albeit not essential, for tyrosine import. Using a combination of metabolomics and heterologous expression, we confirmed a primary role in tyrosine import for *ApiAT5-3*. However, no significant differences in tyrosine import could be detected in phosphorylation site mutants showing

that if tyrosine transport is affected by S56 phosphorylation, its regulatory role is subtle.

Introduction

The fast-growing tachyzoite stage of the protozoan parasite *Toxoplasma gondii* requires cycles of host cell invasion, replication and lysis for its successful proliferation within the host. Each step of this lytic cycle involves tightly regulated signalling pathways, the intricacies of which remain largely unknown. Paramount to parasite survival is the ability to sense and respond to changes in the environment for which the divalent calcium ion (Ca^{2+}) acts as an important secondary messenger (Lourido and Moreno, 2015). Changes in free intracellular $[\text{Ca}^{2+}]_i$ levels, via release of Ca^{2+} from organellar Ca^{2+} stores, can be induced by the addition of Ca^{2+} ionophores, such as A23187 or phosphodiesterase inhibitors (Sidik, Hortua Triana, *et al.*, 2016; Stewart *et al.*, 2016). Ca^{2+} flux regulates key processes including secretion of micronemes prior to host cell entry (Carruthers and Sibley, 1999), parasite motility (Wetzel *et al.*, 2004), and host cell egress (Endo *et al.*, 1982) and invasion (Lovett and Sibley, 2003). Inversely, these processes can all be inhibited by Ca^{2+} immobilisers or chelators, such as BAPTA-AM (Mondragon and Frixione, 1996; Black *et al.*, 2000; Moudy *et al.*, 2001; Wetzel *et al.*, 2004). Ca^{2+} release leads to the activation of Ca^{2+} -binding proteins such as calmodulins, calcineurin B-like kinases and calcium-dependent protein kinases (CDPKs). *T. gondii* calcium-dependent protein kinase 3 (*TgCDPK3*), for example, has been implicated in the regulation of ionophore-induced egress, IIE (i.e. the rapid exit of tachyzoites from a host cell on addition of ionophore) and ionophore-induced death, IID (i.e. the loss of infectivity of extracellular parasites after prolonged exposure to ionophore) (Black *et al.*, 2000). *TgCDPK3* KO ($\Delta cdpk3$) (McCoy *et al.*, 2012), mutants (Black *et al.*, 2000) and chemically inhibited *TgCDPK3* lines (Lourido *et al.*, 2012) all show a deficiency in IIE and IID. *TgCDPK3* is a serine/threonine kinase belonging to a large family of CDPKs also found in plants and ciliates, but absent in humans. It is anchored to the parasite plasma membrane, via N-terminal myristoylation and palmitoylation motifs (Garrison *et al.*, 2012; Lourido *et al.*,

Accepted 20 October, 2018. *For correspondence. E-mail Moritz.treeck@crick.ac.uk; Tel. +44 20 3796 2345.

© 2018 The Authors. Molecular Microbiology Published by John Wiley & Sons Ltd.

This is an open access article under the terms of the Creative Commons Attribution License, which permits use, distribution and reproduction in any medium, provided the original work is properly cited.

2012; McCoy *et al.*, 2012), facing the lumen of the parasite. Like all CDPKs, *TgCDPK3* possesses a C-terminal calmodulin-like domain that consists of EF hands, known as the CDPK activation domain, as well as upstream auto-inhibitory and catalytic domains (Huang *et al.*, 1996; Billker *et al.*, 2009). Binding of Ca^{2+} to the EF hands causes a structural rearrangement that frees up the active site of the kinase domain, allowing for substrate phosphorylation (Wernimont *et al.*, 2010, 2011). A quantitative phosphoproteome study revealed 156 phosphorylation sites that are differentially phosphorylated between WT and *TgCDPK3* mutant parasites (Treeck *et al.*, 2014). The *TgCDPK3*-dependent phosphoproteome includes phosphorylation sites on proteins involved in parasite motility, such as the cyclase-associated protein and myosin A (Myo A), but also, and perhaps surprisingly, those involved in metabolic processes such as the α -ketoacid dehydrogenase (BCKDH) subunit, E1 α , required for the breakdown of branched-chain amino acids (BCAAs) and conversion of pyruvate to the TCA driver acetyl-CoA (MacRae *et al.*, 2012; Oppenheim *et al.*, 2014). The link to proteins not obviously involved in egress and motility, as well as changes in the phosphoproteome regardless of the presence of ionophore, suggests that *TgCDPK3* function extends beyond egress.

The phosphorylation site that appeared to have one of the most marked reductions in phosphorylation state in *TgCDPK3* mutants compared to WT parasites (Treeck *et al.*, 2014), is situated within a putative transporter of the MFS family (TGGT1_257530, named ApiAT5-3 as per Parker *et al.*, 2018) that has moderate homology to a BCAA transporter. Given the additional evidence from the phosphoproteomic dataset that *TgCDPK3* putatively regulates BCAA catabolism via BCKDH, we hypothesised that *TgCDPK3* might be involved in BCAA uptake in addition to regulating motility. Through functional analysis, we show that ApiAT5-3 is rapidly phosphorylated at serine 56 (S56) during the first minute of induced egress. Using a conditional KO approach, we show that ApiAT5-3 is essential, and that deletion leads to a delayed death phenotype that is accompanied by a transcriptional response relating to translational stress. Using a combination of metabolic analysis and heterologous expression in *Xenopus laevis* oocytes, we confirm that ApiAT5-3 transports tyrosine but has only limited capacity to transport BCAAs. In growth competition assays performed with parasite lines that rely on phosphomutants or phosphomimetics, we show that phosphorylation of S56 may be important, but not essential, for parasite fitness. However, we could not measure significant differences in tyrosine import using metabolomic or heterologous expression assays of phosphorylation site mutants. This suggests that

either *TgCDPK3*-mediated phosphorylation is not important for ApiAT5-3 function, or that the effect is too subtle to measure and plays a small contribution to the phenotypes observed for *TgCDPK3* inactivation.

Results

ApiAT5-3 is located at the parasite periphery and phosphorylated during ionophore-induced egress in a *TgCDPK3*-dependent manner

ApiAT5-3 was previously identified as phosphorylated at serine 56 in a *TgCDPK3*-dependent manner (Treeck *et al.*, 2014). BLAST analysis using the Transporter Classification Database (<https://www.tcdb.org/>) predicts that ApiAT5-3 possesses a modest level of homology to a BCAA transporter. This was interesting, as deletion of *TgCDPK3* was previously shown to lead to upregulation of the BCKDH complex (Treeck *et al.*, 2014), involved in BCAA catabolism. This indicated that *TgCDPK3* may directly control BCAA transport by phosphorylating ApiAT5-3.

Topology prediction (https://embnet.vital-it.ch/software/TMPRED_form.html, Hofmann, 1993) places the N-terminal regions of ApiAT5-3 at the luminal side of the parasite, potentially allowing for direct interaction with *TgCDPK3*, which also localises to the plasma membrane. ApiAT5-3 contains several phosphorylation sites at its N-terminus, of which S56 was the only one previously identified as being *TgCDPK3*-dependent (Fig. 1A, upper panel). It is entirely plausible, however, that kinases other than *TgCDPK3* act during egress to phosphorylate additional residues on the ApiAT5-3 N-terminus. To investigate this, we queried a dataset recently generated in our laboratory in which we have quantified, using tandem-mass-tag technology (Thompson *et al.*, 2003), phosphorylation site abundance on *T. gondii* proteins across four time points (0, 15, 30 and 60 s) following ionophore treatment (Caia Dominicus, in preparation). From the ~850 phosphorylation sites that are phosphorylated or dephosphorylated during egress, we identified S56 of ApiAT5-3 as increasingly phosphorylated over time (Fig. 1A, lower panel, Table S1). We also identified several proteins already known to be more phosphorylated in response to Ca^{2+} signalling including Myosin A, Myosin F and DrpB (Nebl *et al.*, 2011; Lourido *et al.*, 2013; Treeck *et al.*, 2014). None of the other phosphorylation sites on the ApiAT5-3 N-terminus increased in phosphorylation state prior to, or during egress (Table S1). However, S15 of ApiAT5-3 was dephosphorylated during ionophore treatment. Collectively these data indicate that S56 is phosphorylated in a *TgCDPK3*-dependent manner upon Ca^{2+} stimulation, and that a phosphatase is acting on S15 during the same period, while the other phosphorylation

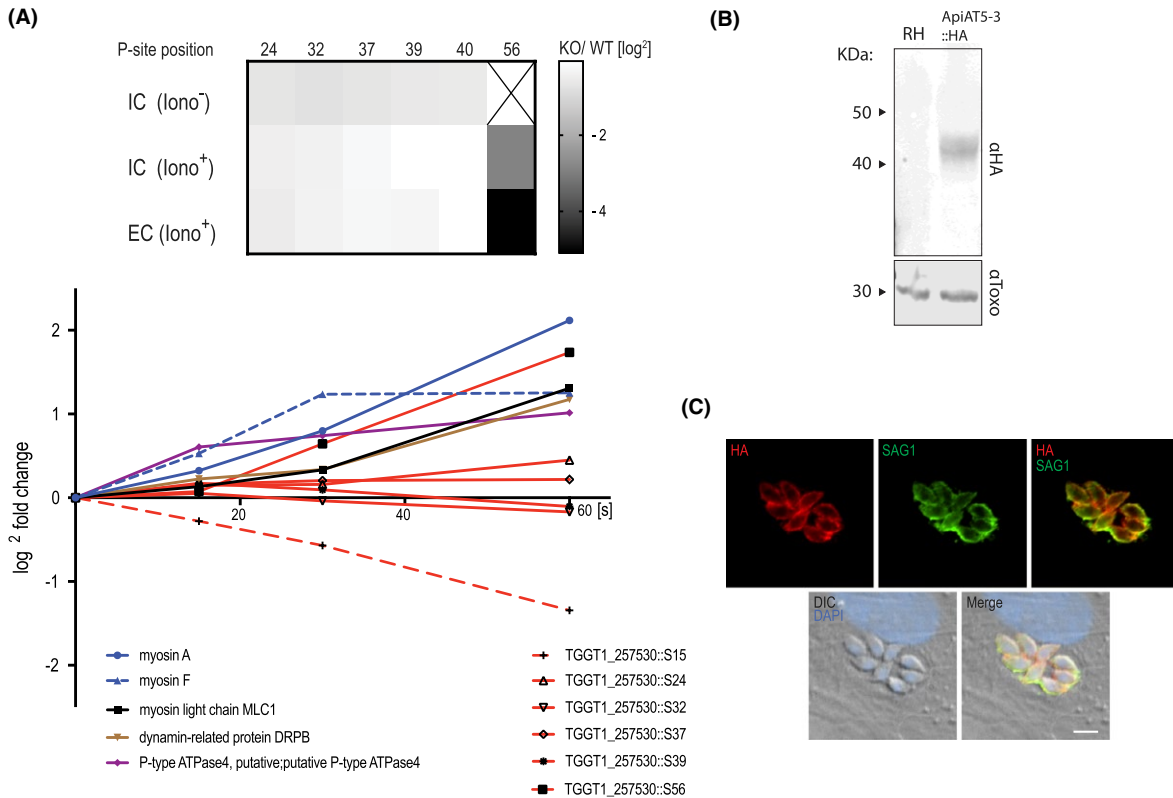


Fig. 1. ApiAT5-3 localises to the plasma membrane and is phosphorylated at serine 56 upon ionophore treatment.

A. Quantification of the phosphorylation state of residues in the ApiAT5-3 N-terminus in *TgCDPK3* KOs and during ionophore-induced egress (from Trecek *et al.*, 2014). Upper panel: The heatmap shows differential phosphorylation of S56 in *TgCDPK3* mutants compared to WT parasites, but not any other of the identified phosphorylation sites. Intracellular (IC) and extracellular (EC) parasites with and without 1 μM ionophore (iono). P-site = phosphorylation site. Numbers represent residue position. Black 'x' = phosphorylation site not identified. Fold changes are log². Bottom panel: Change in relative phosphorylation of ApiAT5-3 and proteins with previously described ionophore-dependent phosphorylation sites, measured after addition of 8 μM ionophore over 60 s. Numbers after the identifier represent the phosphorylation site quantified.

B. ApiAT5-3 was detected by Western blot analysis of ApiAT5-3::HA cell lysate using an anti-HA antibody. Loading control anti-Toxo.

C. IFA of ApiAT5-3::HA expressing parasites shows that ApiAT5-3 localises to the periphery of the intracellular tachyzoite. Red = HA, Green = SAG1, Blue = DAPI. Scale bar = 5 μm.

sites either remain unaffected or are not detected by the assay.

To localise ApiAT5-3 in *T. gondii* parasites, we introduced an ectopic copy of the *apiAT5-3* gene with a HA-epitope tag at its C-terminal, into RH Δ *hxgprt* parasites (ApiAT5-3::HA). 1000 bp upstream of the start-ATG were used as a predicted promotor to ensure natural expression levels. Western blotting confirmed expression of a 42 kDa protein close to the predicted size (56 kDa) (Fig. 1B). Immunofluorescence assays (IFA) showed ApiAT5-3 at the periphery of the parasite, co-localising with SAG1 that resides at the plasma membrane (Fig. 1C). No ApiAT5-3::HA could be detected in nascent daughter cells, a hallmark of most inner membrane complex proteins. Together, these data suggest that ApiAT5-3 localises, like *TgCDPK3*, to the plasma membrane, and thus, could be a *bona fide* target of *TgCDPK3* *in vivo*.

apiAT5-3 deletion causes delayed parasite death

ApiAT5-3 depletion is predicted to have a high fitness cost (Toxo DB 7.1 [Sidik, Huet, *et al.*, 2016]). Accordingly, we generated a conditional KO using the dimerisable cre recombinase (DiCre) strategy. We replaced the endogenous copy of *apiAT5-3* with a recodonised version in RH Δ *ku80*^{DiCre} parasites, by double homologous recombination, using a double-guide strategy (Long *et al.*, 2016) (Fig. 2A). We initially placed a loxP site adjacent to the Kozac sequence of ApiAT5-3 but were unable to obtain correct integration. We hypothesised that the loxP sequence might be interfering with promotor elements and moved it 100 and 200 bp upstream of the predicted start ATG respectively. Both of these constructs correctly integrated into the genome. Subsequent analyses were performed with the resulting ApiAT5-3_loxP, with the loxP at ATG -100bp. Integration was confirmed by PCR amplification (Fig. 2B, left panel). To test whether ApiAT5-3 is

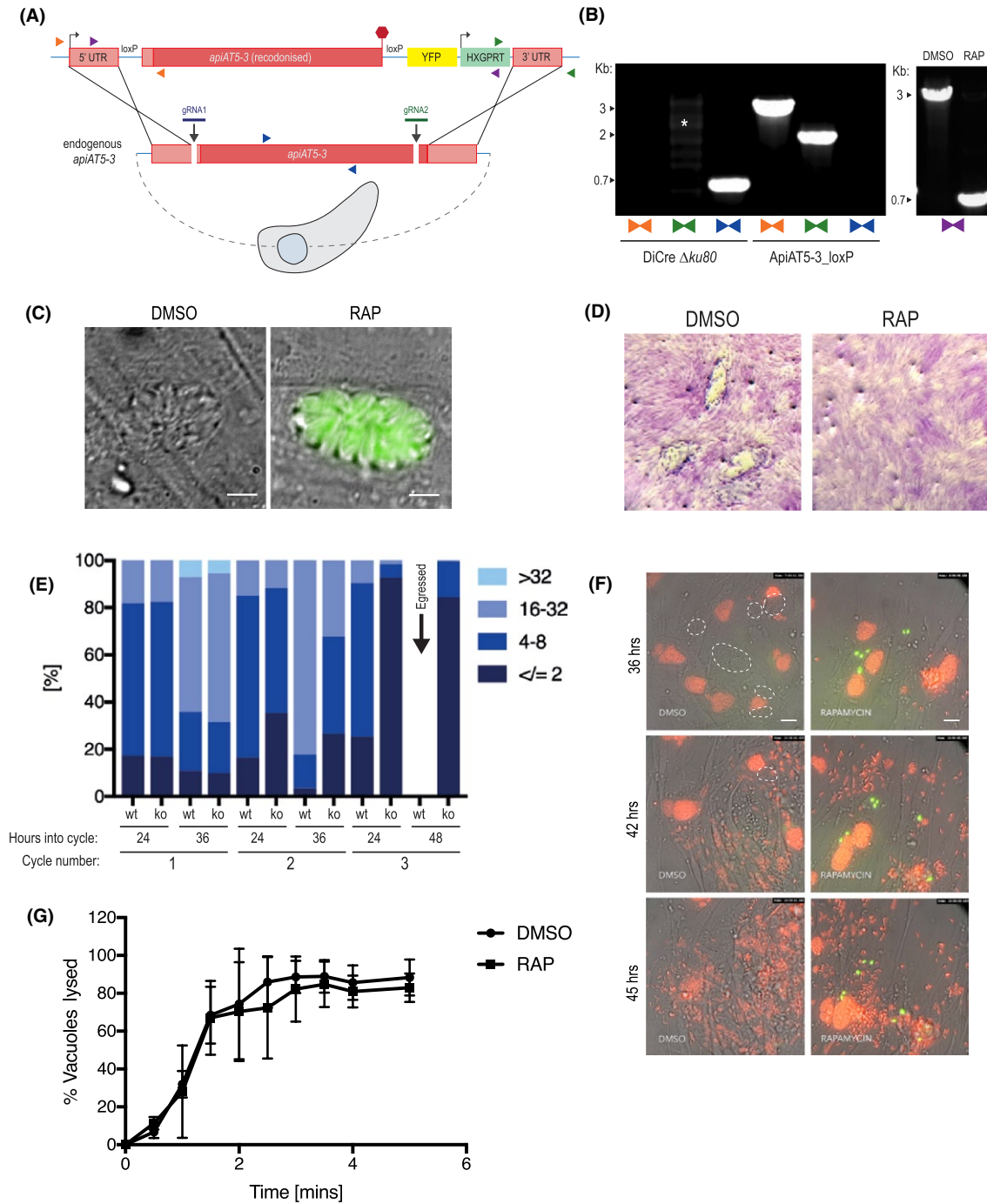


Fig. 2. *ApiAT5-3* is essential for parasite proliferation.

A. Generation of the *ApiAT5-3_loxP* line using CRISPR/Cas9 to increase site-directed integration. Protospacer adjacent motif (PAM) indicated by black arrows. Primer pairs represented by coloured triangles.

B. Left panel: PCR analysis shows correct integration of the *ApiAT5-3_loxP* construct at both the 3' and 5' ends and a loss of WT *apiAT5-3* at the endogenous locus. White * = non-specific bands. Right panel: Addition of RAP leads to correct recombination of the loxP sites.

C. Fluorescent microscopy of *ApiAT5-3_loxP* parasites 24 h after addition of DMSO or RAP. Scale bar 5 μm.

D. Plaque assay showing loss of plaquing capacity of *ApiAT5-3_loxP* parasites upon RAP treatment.

E. Parasite per vacuole number shown as mean %, $n = 3$.

F. Stills from live video microscopy at 36, 42 and 45 h into third lytic cycle post-RAP treatment. Red = RH Tom, dashed white line = intact WT *ApiAT5-3_loxP* vacuoles, green = *apiAT5-3* KO. Scale bar 20 μm.

G. IIE assay showing no significant difference between DMSO- and RAP-treated *ApiAT5-3_loxP* (at 30 h into lytic cycle 2 post-DMSO/RAP treatment). Statistical analysis using multiple comparison two-way ANOVA, $n = 2$.

an essential gene, we treated parasites for 4 h with either rapamycin (RAP) or DMSO. PCR analysis showed a near complete excision of the floxed gene (Fig. 2B, right panel). Correct excision of the *ApiAT5-3* open reading frame resulted in YFP positive parasites that could be readily distinguished from WT by microscopy (Fig. 2C). Upon performing plaque assays it became evident that RAP, but not DMSO treatment, resulted in a complete block in plaque formation (Fig. 2D). A small number (<0.5%) of plaques could be identified in RAP-treated cultures, however, parasites contained in these plaques were YFP(-), indicating that they arose from non-excised parasites (data not shown). Over time these non-excised parasites within the RAP-treated population outgrew the KOs (Fig. S1A), further reinforcing the fact that *ApiAT5-3* is essential for parasite survival under these experimental conditions. These non-excising parasites (termed *ApiAT5-3_loxP^{dDiCre}*) were isolated and, even on the addition of subsequent RAP, did not lose their endogenous copy of the gene (Fig. S1B). These *ApiAT5-3_loxP^{dDiCre}*, which presumably possess a non-functioning diCre recombinase, were used as controls for subsequent experiments, as detailed below. In an attempt to isolate *apiAT5-3* KOs and generate stable Δ *apiAT5-3* lines, YFP (+) parasites were sorted by flow cytometry. However, neither sorting for a population of excised, YFP (+) parasites using fluorescence-activated cell sorting (FACS), nor single-cell cloning by limiting dilution after RAP-mediated excision, resulted in viable parasites. Although small plaques in cloning plates were initially visible under the microscope after 9 days (Fig. S1C), they did not grow any further, suggesting that *apiAT5-3* KO leads to eventual parasite death rather than a maintenance of growth at low levels.

To visualise at which time points *ApiAT5-3* is important, we followed replication of live RAP-treated *ApiAT5-3_loxP* parasites over three lytic cycles, where each lytic cycle is defined as growth over 36 h, before passage into a fresh culture dish containing host cells. This analysis revealed that in the first cycle, RAP-treated (*apiAT5-3* KO) parasite numbers and replication rate remained comparable to DMSO-treated (WT) parasites (Fig. 2E). However, by 36 h into the second replicative cycle there was a 60.7% decrease in the number of vacuoles with more than 16 parasites compared to the DMSO control. By the end of the third cycle the *apiAT5-3* KO parasites consisted largely of two or fewer parasites/vacuole, even after the WT had successfully egressed (48 h into cycle). To better identify phenotypic consequences of *apiAT5-3* deletion, we followed replication over time using live-video microscopy. We started recording 29 h into the third lytic cycle post-RAP treatment, by which time *apiAT5-3* KO parasites display a marked growth defect. To facilitate a more accurate comparison between *apiAT5-3* KO and WT parasites, tdTomato expressing RH parasites (RH Tom)

were spiked into the imaging wells at a 1:1 ratio. These analyses revealed that *apiAT5-3* KO does not lead to early egress. However, in the subsequent parasite cycle parasites that invade often do not proceed beyond two parasites/vacuole (Fig. 2F, Movies S1A and B).

As we showed that *ApiAT5-3* is phosphorylated directly after ionophore treatment (Fig. 1A), we postulated that it may be required for IIE. To assess this, we performed egress assays of the DMSO- and RAP-treated lines in the presence of 8 μ M Ca^{2+} ionophore. However, there was no significant difference between the KO and WT (Fig. 2G) suggesting that phosphorylation of *ApiAT5-3*, in response to elevated Ca^{2+} levels, plays a role in processes other than egress.

apiAT5-3 deletion causes upregulation of genes encoding for ribosome subunits, but not alternative transporters

Deletion of a transporter may lead to upregulation of alternative transporters or may manifest as a stress response that carries a detectable signature. To investigate this, we measured transcript levels using RNA-seq, comparing RAP-treated *ApiAT5-3_loxP* with *ApiAT5-3_loxP^{dDiCre}* parasites, which, as mentioned previously, do not excise the endogenous locus, even when treated with RAP (Fig. S1B). RNA was isolated in biological triplicate at 4 h post-RAP treatment, the time point at which we did not expect to see major changes in the transcriptome, and 60 h post-treatment, by which time point the RAP-treated *ApiAT5-3_loxP* parasites are still viable but start to display a growth defect. Indeed, at 4 h transcripts from the *apiAT5-3* gene were only slightly reduced in the RAP-treated *ApiAT5-3_loxP* parasites compared to the RAP-treated *ApiAT5-3_loxP^{dDiCre}* parasites (17.1%). In contrast, at 60 h post-RAP treatment, a 64.7% reduction was observed (Fig. 3A). Unexpectedly, only 435 transcripts showed a statistically significant differential expression between the WT and *apiAT5-3* KO parasites at the 60 h time point, compared to the 4 h time point, indicating a modest transcriptional response to *apiAT5-3* deletion (Fig. 3B). GO-term analysis of the differentially transcribed genes showed most enrichment (5.41-fold) for genes important for translation. Among this enriched group, these genes encode almost exclusively genes for ribosomal proteins (Fig. 3C, Table S2). No single transporter was specifically upregulated, indicating that there is no rapid transcriptional compensation when *apiAT5-3* is deleted.

Collectively these data show that *ApiAT5-3* is an essential protein that is required for intracellular replication. Its depletion leads to a complete arrest in growth which is not accompanied by a substantial stress response, but rather modest signs of translational stress.

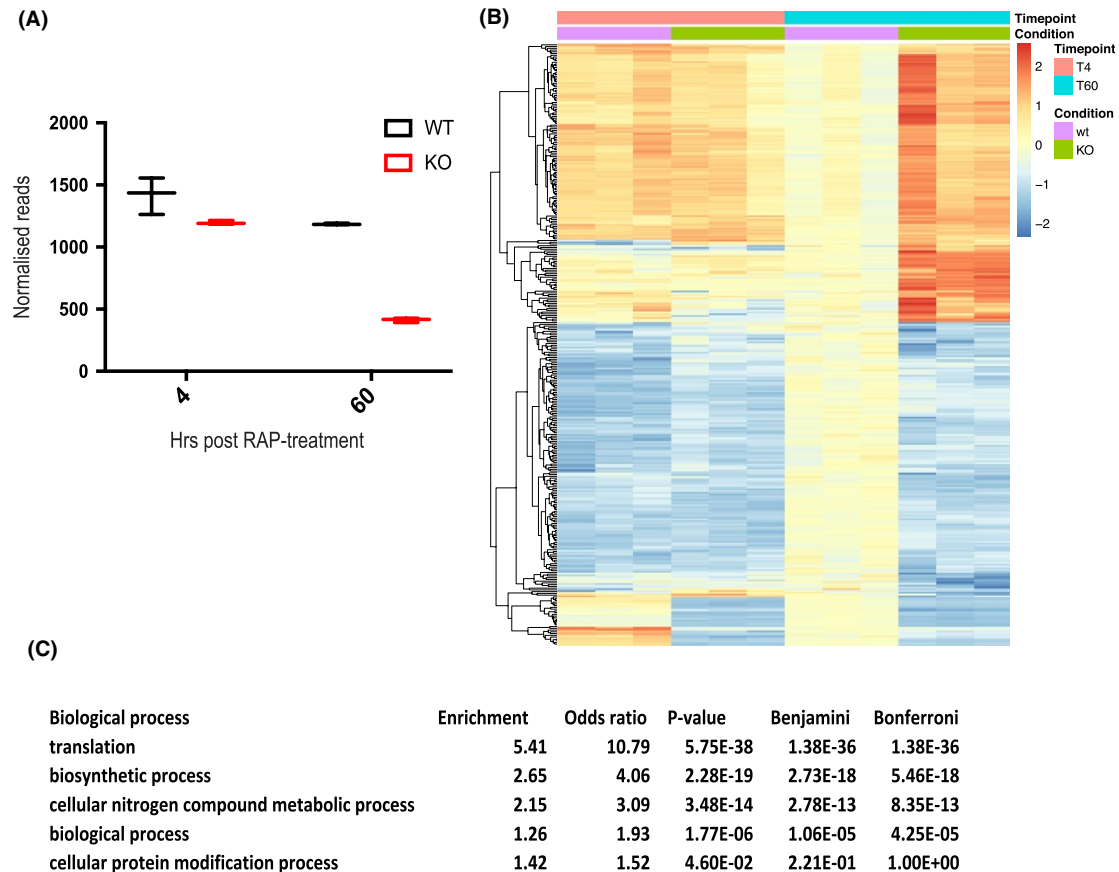


Fig. 3. $\Delta apiAT5-3$ parasites display a transcriptional response related to amino acid starvation.

A. Extracted reads for recodonised *apiAT5-3* from RNA sequence data show a significant reduction of *apiAT5-3* transcripts in RAP-treated *ApiAT5-3_loxP* lines 60 h post-RAP treatment compared to RAP-treated *ApiAT5-3_loxP^{dICre}* parasites.

B. Heatmap of genes that change significantly (adjusted $p < 0.05$) in transcript read number between WT and $\Delta apiAT5-3$ 60 h post-addition of RAP.

C. Gene ontology term enrichment shows that genes involved in translation processes are significantly enriched among the differentially expressed genes 60 h post-RAP treatment.

Mutation of S56 to alanine, but not a phosphomimetic leads to a reduction in fitness

Having established that *ApiAT5-3* is essential for the lytic cycle, we next sought to examine the role of *TgCDPK3*-mediated phosphorylation in *ApiAT5-3* function. To do this, we complemented *ApiAT5-3_loxP* parasites with either WT *ApiAT5-3*, or variants where S56 is mutated to alanine (S56A) or to aspartic acid (S56D). To prevent possible differences in growth between the parasite lines due to differential expression of the complementation constructs, we inserted each into the *uprt* locus by double homologous recombination, under control of the endogenous promoter (Fig. 4A). Complementation into the *uprt* locus was verified by PCR (Fig. 4B). The complementation constructs also carried a C-terminal HA epitope tag to verify correct trafficking to the plasma membrane. Immunofluorescence displayed correct trafficking in all variants (Fig. 4C).

To compare fitness between the WT, the phosphomimetic (S56D) and the phosphomutant (S56A) complemented lines in the absence of *apiAT5-3*, we deleted the endogenous copy using RAP treatment. This results in parasite strains that solely rely on the complemented copy of the gene. We confirmed correct excision of *apiAT5-3* by virtue of YFP expression post-RAP treatment (Fig. 4C) and PCR analysis (Fig. S2A). To ensure protein levels of the complemented genes were comparable, we attempted to quantify protein levels of the $\Delta apiAT5-3^{ApiAT5-3}$, $\Delta apiAT5-3^{ApiAT5-3_{S56A}}$ and $\Delta apiAT5-3^{ApiAT5-3_{S56D}}$ lines by Western blot. However, despite several attempts, we failed to visualise the complemented proteins. As an alternative approach, we sought to quantify the protein levels using fluorescent anti-HA antibodies and analysis by flow cytometry. Comparison of the geometric mean of fluorescence indicated that the amount of *ApiAT5-3*, *ApiAT5-3_{S56A}*

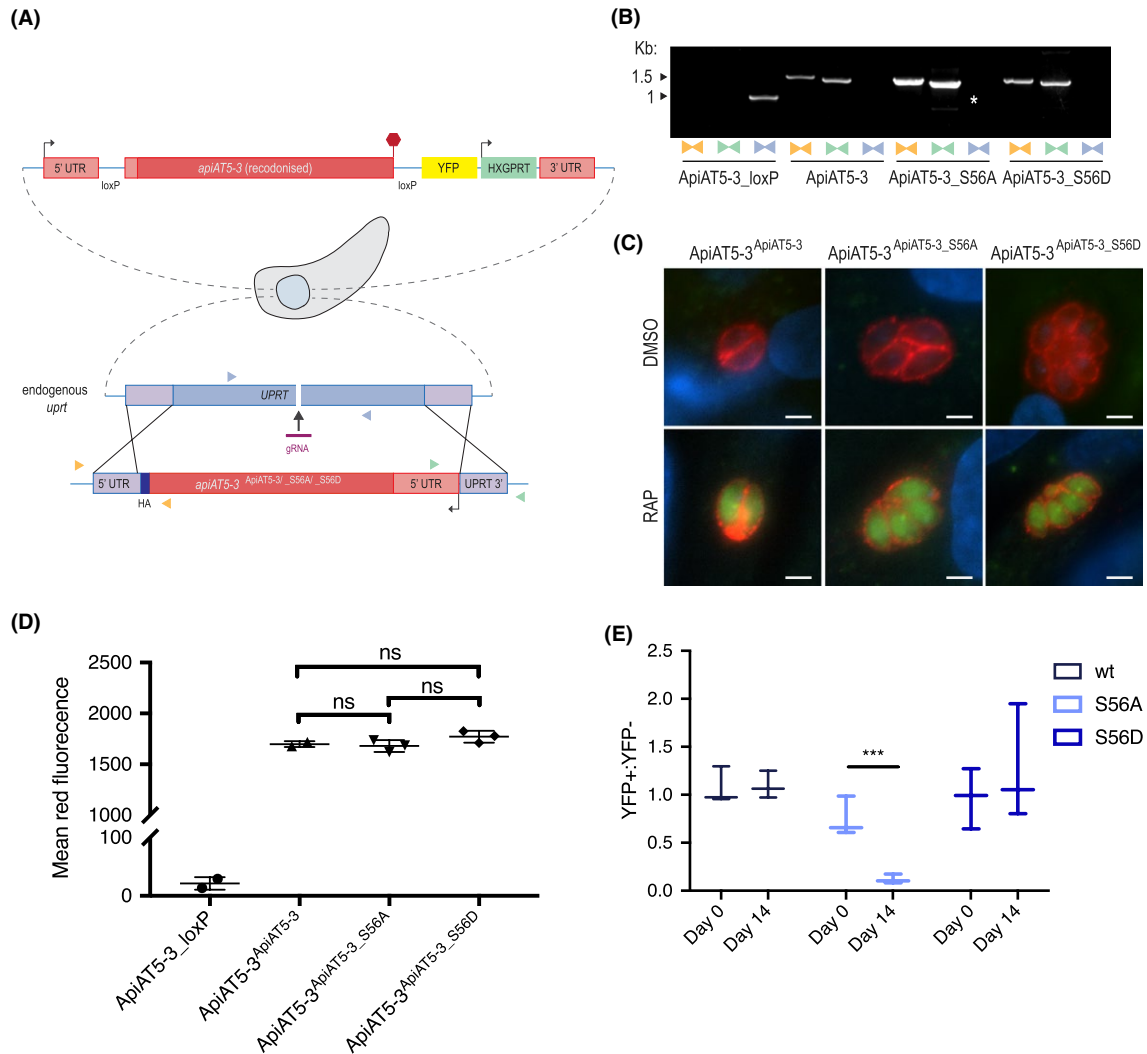


Fig. 4. Δ *apiAT5-3*^{ApiAT5-3_S56A} demonstrates a fitness defect.

A. Generation of the *ApiAT5-3*^{ApiAT5-3/_S56A/_S56D} complementation lines. PAM indicated by black arrow. Primer pairs represented by coloured triangles.

B. PCR analysis shows correct integration of the *ApiAT5-3_loxP* construct at both the 3' and 5' ends and a loss of *uprt*. White * = nonspecific band.

C. IF of *ApiAT5-3*^{ApiAT5-3/_S56A/_S56D::HA} expressing parasites shows that *ApiAT5-3* is correctly trafficked to the periphery of the intracellular tachyzoite in both the presence (DMSO) and absence (RAP) of the endogenous *apiAT5-3*. Red = HA. Green = YFP, indicating correct excision of the endogenous *apiAT5-3*. Scale bar 10 μ m.

D. Geometric mean of red fluorescence calculated by flow cytometric analysis of complemented parasites, probed with red fluorescent anti-HA antibody. Statistical analysis carried out using multiple comparison, two-way ANOVA, ns = not significant. All complemented lines differ significantly in mean fluorescence from *ApiAT5-3_loxP* ($p < 0.0001$), $n = 3$.

E. Growth competition assay by flow cytometry shows that Δ *apiAT5-3*^{ApiAT5-3_S56A} parasite growth is reduced relative to the non-excised *ApiAT5-3*^{ApiAT5-3_S56A} line. Statistical analysis using multiple comparison, two-way ANOVA of mean ratio to day 0 normalised to 1.

*** $p < 0.001$, $n = 3$.

or *ApiAT5-3_S56D* protein did not differ significantly between the complemented lines (Fig. 4D). This would suggest that any subsequent phenotypes were a result of mutation of the S56 phosphorylation site and not differing *apiAT5-3* expression levels. RAP-treated parasite lines were viable and allowed us to isolate clones by limiting dilution, all of which restored growth in plaque assays (Fig. S2B). This shows that (i) complementation of *apiAT5-3* by expression at the *uprt* locus fully restores

ApiAT5-3 function and (ii) that neither the introduction of phosphomimetics nor phosphomutants of S56 are lethal to parasite growth. This is not surprising as deletion of *TgCDPK3*, the kinase putatively responsible for *ApiAT5-3* phosphorylation during egress, does not lead to a severe growth phenotype. Accordingly, phosphomutants would not be expected to display drastic differences in growth. We therefore performed competition assays in which we compared growth of YFP expressing

complementation lines that fully rely on the complementation variant for growth ($\Delta\text{apiAT5-3}^{\text{ApiAT5-3/S56A/S56D}}$) mixed in a 1:1 ratio with their non-excised, colourless counterpart ($\text{ApiAT5-3}^{\text{ApiAT5-3/S56A/S56D}}$). Using the ratio of 4',6-diamidino-2-phenylindole (DAPI)-stained parasites (DAPI labels the DNA of all parasites) and YFP expressing parasites (YFP is expressed only in the complementation lines), we followed growth over 14 days in biological triplicates. While $\Delta\text{apiAT5-3}^{\text{ApiAT5-3}}$ parasites showed no difference in growth compared to their WT control, $\Delta\text{apiAT5-3}^{\text{ApiAT5-3_S56A}}$ was reduced by 84.0% after 14 days (Fig. 4E). Strikingly, $\Delta\text{apiAT5-3}^{\text{ApiAT5-3_S56D}}$ was not outcompeted and grew at similar levels to the WT control.

Collectively these data indicate that phosphorylation of S56 while not essential is important for intracellular growth. However, we cannot exclude that mutating S56 to an alanine impacts protein function by other means than mimicking non-phosphorylated S56.

ApiAT5-3 is a primary transporter of tyrosine, but not branched-chain amino acids

The predicted homology of *ApiAT5-3* to a BCAA transporter and the profound upregulation of the BCKDH complex in Δcdpk3 parasites suggested a direct role for *ApiAT5-3* in BCAA transport. To test this, we expressed *apiAT5-3* in the heterologous expression system, *X. laevis* oocytes. Concurrently with our study, data were presented that *ApiAT5-3* may be a tyrosine transporter (Giel van Dooren, personal communication and pre-published in BioRx [Parker *et al.*, 2018]). We, therefore, tested BCAA import and replicated the tyrosine uptake capacity of *ApiAT5-3* in oocytes expressing WT *ApiAT5-3* (Fig. 5A). Measuring unidirectional influx, we observed a significant (4.0-fold) increase in the uptake of ^{14}C -tyrosine into *ApiAT5-3*-expressing oocytes compared to either water-injected or uninjected control oocytes under the conditions tested, consistent with results from (Parker

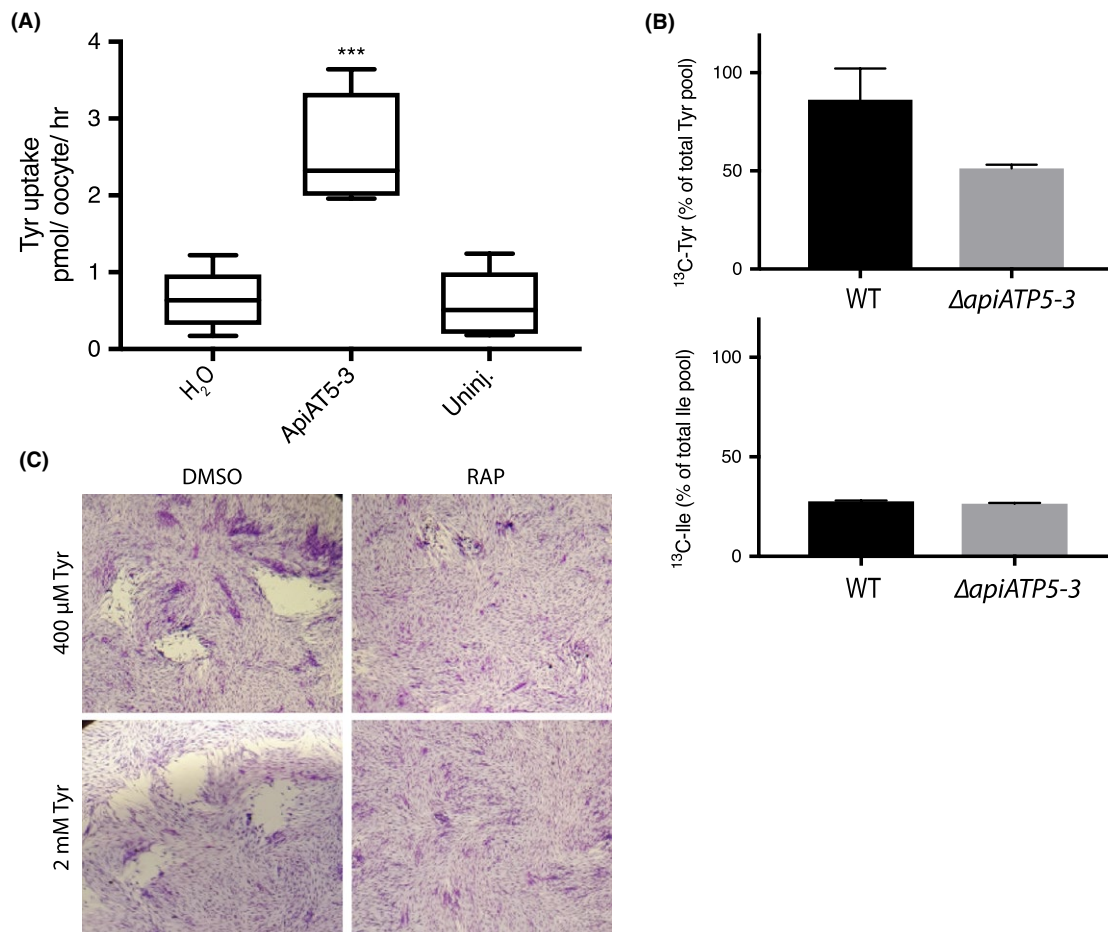


Fig. 5. Functional analysis of the *ApiAT5-3* transporter.

A. *X. laevis* oocytes expressing *ApiAT5-3* demonstrate a significant increase in ^{14}C -L-tyrosine uptake. Ten oocytes per experiment.

Analysis carried out using a two-tailed, paired, Student's *t*-test. ****p* < 0.001 Box plots show mean, first and third quartile and SD, *n* = 5.

B. Extracellular, RAP-treated, *ApiAT5-3_loxP* tachyzoites, labelled with ^{13}C -L-tyrosine or ^{13}C -L-isoleucine, display a marked decrease in tyrosine but not isoleucine import, relative to WT, *n* = 2.

C. Plaque assay shows no rescue of growth of RAP-treated *ApiAT5-3_loxP* on addition of excess (2 mM) L-tyrosine.

et al., 2018). We also observed moderate ApiAT5-3-dependent phenylalanine influx, but not for the BCAA valine (Fig. S3A), suggesting that, while ApiAT5-3 is capable of tyrosine transport, it is unlikely to be a major BCAA transporter.

To verify the role of ApiAT5-3 in tyrosine transport in our conditional KO parasites, we measured intracellular ^{13}C -tyrosine levels in RAP-treated $\Delta\text{apiAT5-3}^{\text{ApiAT5-3}}$ (WT) and ApiAT5-3_loxP (KO) parasites (74 h post-excision), after 1 h in the presence of growth media containing ^{13}C -tyrosine. In an analogous manner, we also measured ^{13}C -isoleucine uptake in order to verify if ApiAT5-3 is also a BCAA transporter. $\Delta\text{apiAT5-3}^{\text{ApiAT5-3}}$ was used instead of DMSO-treated ApiAT5-3_loxP to control for any potential effects of RAP on parasite metabolism. This analysis verified a reduction of ^{13}C -labelled tyrosine uptake (40.5% compared to $\Delta\text{apiAT5-3}^{\text{ApiAT5-3}}$), but not isoleucine uptake (4.3% compared to $\Delta\text{apiAT5-3}^{\text{ApiAT5-3}}$) (Fig. 5B). We also measured the intracellular abundance of all detectable amino acids when labelling with ^{13}C -tyrosine. We observed a reduction of intracellular tyrosine abundance (63.2%) in the *apiAT5-3* KO cells (as expected), but not phenylalanine which was slightly increased in relative abundance (17.45%), suggesting that while ApiAT5-3 is able to transport phenylalanine in oocytes, it is not the major phenylalanine transporter in *T. gondii* (Fig. S3B). It is important to note that our metabolome analysis was performed at the end of cycle 2 after RAP treatment, when RAP-treated *apiAT5-3_loxP* parasites are still viable but start to display a reduction of growth (Fig. 2E). Therefore, we predict that low levels of ApiAT5-3 present at this stage are responsible for the residual transport of tyrosine. Interestingly, we also observed a reduction in intracellular aspartate (38.5%) and glycine (28.3%) in *apiAT5-3* KO cells (Fig. S3B). Since *T. gondii* is not known to be auxotrophic for these amino acids, we reasoned that the observed death phenotype is unlikely caused by a defect in glycine or aspartate import, and instead focused our subsequent analysis on tyrosine. We also observed an increase in the abundance of glutamine, valine, isoleucine and proline, indicating potential wider metabolic effects.

To test whether exogenous tyrosine can complement the loss of ApiAT5-3, we grew parasites in media with 5 \times the normal amount of tyrosine (2 mM). However, plaque assays revealed that RAP-treated ApiAT5-3_loxP parasite growth was not restored (Fig. 5C). Several attempts were also made to isolate stable $\Delta\text{apiAT5-3}$ clonal lines by limiting dilution in the presence of 2 mM tyrosine. Again however, this was unsuccessful as parasites appeared to die after several rounds of replication, much like those grown in normal media. In other organisms, phenylalanine can be converted into tyrosine. Therefore, we tested whether phenylalanine supplementation (2 mM) can rescue the

growth phenotype of *apiAT5-3* KO parasites. No growth rescue could be observed (Fig. S3D). Together, these results suggest that ApiAT5-3 is the only transporter of tyrosine in *T. gondii* and that phenylalanine cannot be readily converted into tyrosine in *T. gondii* parasites.

As ApiAT5-3 is phosphorylated during egress in a TgCDPK3-dependent manner, and as S56 phosphomutants display a moderate fitness cost, we postulated a functional link between S56 phosphorylation and tyrosine import. We, therefore, tested uptake of isotopically labelled tyrosine by extracellular $\Delta\text{apiAT5-3}^{\text{ApiAT5-3_S56A}}$ and $\Delta\text{apiAT5-3}^{\text{ApiAT5-3_S56D}}$ phosphomutant strains. No statistically significant difference in tyrosine import was observed in these assays (Fig. S3E) either because phosphorylation of S56 plays no role in tyrosine import, or because the effect of phosphomutations on tyrosine import at the parasite level is subtle. Therefore, we also assessed differences in tyrosine uptake in *X. laevis* oocytes heterologously expressing ApiAT5-3_S56A and ApiAT5-3_S56D. As it has not been determined whether the S56 residue is phosphorylated *in situ* by native oocyte kinases, it is difficult to determine the exact role of phosphorylation in the tyrosine transport function of ApiAT5-3 expressing oocytes. However, comparison between S56A phospho-null to S56D phosphomimic expressing oocytes could provide a good indication as to the functional relevance of this residue. Although ApiAT5-3_S56A-expressing oocytes displayed a trend towards a reduction in tyrosine uptake (average 19.5% reduction in S56A relative to WT ApiAT5-3-expressing oocytes), this difference was not statistically significant (Fig. S3F). The S56D expressing oocytes display a marginal increase in tyrosine uptake of 14.0% that again was not statistically significant. Collectively these data indicate that ApiAT5-3 is a primary tyrosine transporter and that S56 phosphorylation plays only a minor, if any, role in tyrosine import.

Discussion

TgCDPK3 has previously been implicated in controlling distinct biological processes such as gliding motility and metabolism. How these are linked, however, has been unclear. Mutants that display only IIE and IID phenotypes have been identified (Black *et al.*, 2000; Gaji *et al.*, 2015), arguing that TgCDPK3 may be an upstream regulator of both processes. Here we show that upon activation by the Ca^{2+} ionophore A23187, TgCDPK3 leads to an increase in ApiAT5-3 phosphorylation at S56. This occurs at the same time, and to a similar intensity, as other previously identified targets of TgCDPK3 (e.g. serine 21/22 of MyoA) and other kinases involved in signalling (e.g. TgCDPK1). MyoA and ApiAT5-3 are both located at, or close to, the plasma membrane. It

is conceivable that, upon activation, *Tg*CDPK3 phosphorylates proteins at the plasma membrane, some of which are important for motility and others (e.g. transporters) that prepare the parasite for the extracellular milieu. In this study, we demonstrate that the S56 residue becomes rapidly phosphorylated prior to egress in a *Tg*CDPK3-dependent manner. However, the timing of phosphorylation during egress does not appear to be linked to the phenotype of the ApiAT5-3 KO, which stalls growth after invasion of the host cell. The timing of phosphorylation during egress and an apparent role of the transporter during intracellular growth could be explained that phosphorylation prepares the parasite for the extracellular milieu, or for reinvasion. Interestingly, ApiAT5-3 possesses several other phosphorylation sites in its N-terminus, aside from S56, that either do not change in phosphorylation state or, in the case of S15, appear dephosphorylated during induced Ca^{2+} signalling. How S15 dephosphorylation and S56 phosphorylation are controlling ApiAT5-3 function requires further investigation, however it is evident that mutating S56 to a non-phosphorylatable residue markedly reduces parasite fitness, similar to the growth defect observed for *Tg*CDPK3 mutants (McCoy *et al.*, 2012). Phosphorylation of transporters has been shown to regulate affinity, specificity and flux of cargo (Liu and Tsay, 2003; Lee *et al.*, 2007; Ramamoorthy *et al.*, 2010; Tamura *et al.*, 2013; Jang *et al.*, 2014; Aryal *et al.*, 2015). Accordingly, the observed fitness cost in S56A mutants could be indicative of a reduction in tyrosine import, for which the parasite is auxotrophic (Marino and Boothroyd, 2017). It appears that deletion of ApiAT5-3 has little effect during the first two lytic cycles of division, indicating that relatively normal growth rates can be sustained with lower ApiAT5-3 levels. A critical point is reached between the second and third lytic cycles, when parasites are still able to egress, but then fail to develop beyond two parasites/vacuole in most cases. Whether this is because ApiAT5-3 function is critically important shortly after invasion, or whether this is the point at which ApiAT5-3 protein levels are diluted below a critical concentration is not known and further work will be required to answer this question.

While we observed a clear role for ApiAT5-3 in tyrosine transport, expression of the ApiAT5_S56A phosphomutant did not lead to significant changes in tyrosine import in *Toxoplasma* parasites or in *Xenopus* oocytes. Although a small reduction in tyrosine import was observed in *Xenopus* oocytes expressing ApiAT5-3_S56A, the difference is subtle and could be the result of small differences in expression levels or phosphorylation state of ApiAT5-3 in oocytes. Thus, the oocyte assays did not allow us to draw conclusions on the effect of S56 phosphorylation, apart from that it appears not to be a prerequisite for

tyrosine import in *T. gondii*. Whether or not S56 phosphorylation plays a minor role in regulating ApiAT5-3 cannot be answered at this stage. Growth competition assays showed that a phosphomimetic mutant gives parasites a competitive growth benefit. While this could be a result of changing a functionally important residue to a non-related amino acid, it could also be that phosphorylation of S56 plays a small role in ApiAT5-3 regulation. We observed a 84.0% reduction in growth of $\Delta\text{apiAT5-3}^{\text{ApiAT5-3_S56A}}$ mutants compared to WT parasites over 14 days. This translates into a reduced replication rate of 6.74% per 24 h. If this growth defect is a direct result of reduced tyrosine import, we would predict that there only be a 0.56% reduction in import during the 1 h period in which the ^{13}C -tyrosine uptake assays are performed. This difference would be too small to measure with the methods available. The observation that tyrosine transport by ApiAT5-3 appears only marginally affected by *Tg*CDPK3 activity, leaves open the question as to how *Tg*CDPK3 is linked to the changes observed on the phosphoproteome of metabolic enzymes in *Tg*CDPK3 mutants (Treeck *et al.*, 2014). Further work is required to answer this question.

Apart from regulating amino acid transport, phosphorylation of transporters has also been shown to regulate trafficking to the surface (Nissen-Meyer *et al.*, 2011; Rice *et al.*, 2012; Abramian *et al.*, 2014). However, a role for S56 in trafficking is less likely for two reasons: (i) we did not observe any obvious defects in surface translocation of the transporter in parasites and (ii) *Tg*CDPK3 phosphorylates S56 shortly before, or during egress, at which state the transporter is already on the surface. If S56 phosphorylation was important for surface translocation, we would expect this to occur at an earlier stage. However, we cannot exclude the possibility that minor differences in trafficking capacity impact tyrosine transport, resulting in the growth phenotype.

Interestingly, we haven't been able to rescue the effect of *apiAT5-3* loss in our conditional KO parasites through growth in high tyrosine concentrations. These results differ from those in Parker *et al.* whereby growth can, at least partially, be rescued in high tyrosine medium (Parker *et al.*, 2018). One mechanism to counter low tyrosine levels that most organisms possess, is the ability to convert phenylalanine into tyrosine, via the enzyme phenylalanine-4-hydroxylase (AAH). However, the inability to overcome the tyrosine import-related growth defect in ApiAT5-3 conditional KOs through addition of exogenous phenylalanine, indicates that this pathway is not available. Indeed, both isoforms of AAH (AAH1 and AAH2) have recently been shown to be secreted into the host cell during *Toxoplasma* infection, where they would be unable to rescue a tyrosine transporter defect in the plasma membrane (Marino and Boothroyd, 2017; Wang *et al.*, 2017). Another explanation as to why Parker *et al.* have successfully rescued the effects of *apiAP5-3*

deletion through addition of excess tyrosine, could be via the upregulation of alternative transporters. Although a small amount of tyrosine appears to be imported in our *apiAT5-3* KO line (Fig. 5B), this is likely due to the presence of residual ApiAT5-3 protein in the plasma membrane after RAP treatment. Along with our inability to rescue growth upon tyrosine supplementation, we conclude that this residual tyrosine import is unlikely due to an alternative transporter. Further to this, our transcriptomic analysis argues against a rapid sensing and transcriptional compensation for the lack of tyrosine import, so if upregulation of alternative transporters occurs, it will be a slow process. Another explanation may be that slight differences in the genetic background or passage history, and potential epigenetic changes in the parental strains, leads to a difference in capacity for amino acid transport. There is some indication that this may be the case as, in our metabolomics experiments, the ApiAT5-3 deletion showed reduced levels of glycine and aspartic acid in addition to tyrosine, while in Parker *et al.*, other amino acids were observed to be less abundant in addition to tyrosine. We also saw an increase in abundance of some amino acids that differ from Parker *et al.* It may be interesting in the future, to compare our *apiAT5-3* KO with that of Parker *et al.*, and identify any compensatory mechanisms the parasites can use to adjust to tyrosine starvation. Interestingly, deletion of *apiAT5-3* leads to a growth arrest that is not accompanied by major transcriptional responses, but upregulation of most transcripts for ribosomal subunits, which indicate translational changes in response to tyrosine depletion. We have not further pursued this response in this study, but it is reminiscent of the hibernation state in *Plasmodium falciparum*, whereby depletion of isoleucine, an essential amino acid for this parasite, leads to arrest in growth by translational arrest without a major stress response (Babbitt *et al.*, 2012). This would suggest that translational arrest may be a common response among apicomplexan parasites during amino acid starvation.

In summary, we show that ApiAT5-3, a novel *T. gondii* tyrosine transporter, is rapidly phosphorylated in a *TgCDPK3*-dependent manner at S56 prior to, and during egress from the host cell. This *TgCDPK3*-dependent phosphorylation at S56 appears important for parasite fitness based on phosphomimetics and phosphomutants. These results, together with previous studies, support the notion that *TgCDPK3* simultaneously targets several proteins in, or at, the plasma membrane that are implicated in divergent biological processes, such as motility and nutrient homeostasis. If the phosphorylation sites that depend on *TgCDPK3* function each play a small functional role in *T. gondii* biology, as implicated for S56 on ApiAT5-3, the phenotypes observed in $\Delta cdpk3$ parasites may be an accumulation of effects on various proteins, which is likely true for other kinases as well.

Experimental procedures

Parasite culture

T. gondii parasites were cultured in a confluent monolayer of human foreskin fibroblasts (HFFs) maintained in Dulbecco's Modified Eagle Medium (DMEM), GlutaMAX supplemented with 10% foetal bovine serum, at 37°C and 5% CO₂.

Plasmid and parasite strain generation

A comprehensive list of primers and parasite lines used throughout this study are described in Tables S3 and S4 respectively. To generate the epitope tagged ApiAT5-3::HA line, the *apiAT5-3* gene and associated 5' UTR were PCR-amplified from RH *T. gondii* gDNA using the primers 1 and 2 and cloned using Gibson assembly (Gibson *et al.*, 2008) into pGRA::HA::HPT (Saeij *et al.*, 2006), linearised with HindIII and NcoI. 25 µg of the pGRA::ApiAT5-3::HA vector was transfected into RH $\Delta hxcprt$ parasites as previously described (Soldati and Boothroyd, 1993). 16–20 h after transfection, transgenic parasites were selected using 25 µM mycophenolic acid (MPA) and 50 µg/ml xanthine (XAN). To generate the ApiAT5-3_{loxP} conditional KO lines, the *apiAT5-3* 5' UTR was first PCR-amplified from gDNA with primers 3 and 4. This PCR product was inserted, along with the synthetic DNA constructs *loxP_apiAT5-3_loxP_yfp* and *loxP(-100)_apiAT5-3* (see Table S3 for full sequences), by Gibson assembly into pG140::Actin::YFP (Andenmatten *et al.*, 2013) that had been PCR-amplified using primers 5 and 6 to remove the actin gene. Two microgram of the subsequent pG140::ApiAT5-3_{loxP}::YFP plasmid was linearised with ScaI and co-transfected into RH $\Delta ku80\Delta hxcprt$ with pSag1::Cas9-U6::dbl-sgApiAT5-3, in a molar ratio of 1:10. The pSag1::Cas9-U6::dbl-sgApiAT5-3 vector was generated by PCR amplification of the pSag1::Cas9-U6 (Shen *et al.*, 2014) vector using primers 7 and 8 to insert the 5' gRNA (gRNA 1) and 9 and 8 to insert the 3' gRNA (gRNA 2), prior to re-ligation with T4 DNA Ligase (New England Biolabs, Ipswich, MA, USA). gRNA 1 was then amplified using primers 10 and 11 and Gibson cloned into the pSag1::Cas9-U6::sg2ApiAT5-3 that had been linearised with KpnI and XhoI as per (Long *et al.*, 2016). Transgenic parasites were selected using MPA/XAN as described for pGRA::ApiAT5-3::HA. 5' and 3' integration was confirmed using primer pairs 12 and 13, and 14 and 15 respectively. Absence of WT *apiAT5-3* was confirmed using primers 16 and 17. DiCre-mediated *apiAT5-3* excision was induced with the addition of 50 nM RAP to ApiAT5-3_{loxP} parasites for 4 h. Excision was confirmed using primers 13 and 16. To introduce an ectopic copy of *apiAT5-3* into the *uprt* gene locus, the *apiAT5-3* gene, and associated 5' UTR, were PCR-amplified from gDNA using primers 18 and 19 which was then inserted into the BamHI/ PaeI digested pUPRT::DHFR-D vector (Addgene plasmid #58258 [Shen *et al.*, 2014]) using Gibson assembly. To generate the pUPRT::ApiAT5-3_{S56A}::HA and pUPRT::ApiAT5-3_{S56D}::HA vectors,

the pUPRT::ApiAT5-3::HA vector was modified by site directed mutagenesis using the primers 20 and 21 (S56A) or 22 (S56D). pUPRT::ApiAT5-3::HA, pUPRT::ApiAT5-3_S56A::HA and pUPRT::ApiAT5-3_S56D::HA were linearised with PciI prior to the co-transfection of 2 µg into RH $\Delta ku80\Delta hxppt$ ApiAT5-3_loxP with pSag1::Cas9-U6::sgUPRT (Addgene plasmid #54467 [Shen *et al.*, 2014]) in a molar ratio of 1:10. Transgenic parasites were selected by the addition of 5 µM 5'-fluoro-2'-deoxyuridine to culture medium, 16–20 h post-transfection. Integration into the genome was confirmed using primer pairs 23 and 24, and 25 and 26 respectively. Absence of *uprt* was confirmed using primers 27 and 28.

Western blotting and immunofluorescent imaging

For Western blot analysis, intracellular parasites were lysed in Laemmli buffer (60 mM Tris-HCl pH6.8, 1% SDS, 5% glycerol, 5% b-mercaptoethanol, 0.01% bromophenol blue) and heated to 37°C for 30 min prior to separation on a 10% sodium dodecyl-polyacrylamide gel. Proteins were transferred onto a nitrocellulose membrane prior to blocking in 3% milk, 0.1% Tween-20 PBS. HA-tagged ApiAT5-3 was detected using rat anti-HA (1:500), followed by goat anti-rat LI-COR secondary antibody (1:1500) and visualised with a LI-COR Odyssey scanner. Loading control visualised with Abcam mouse anti-Toxo (1:1000), followed by goat anti-mouse LI-COR secondary antibody (1:1500).

IFA's were performed on intracellular parasites grown in HFFs on glass coverslips. 1×10^5 parasites were seeded 24 h prior to fixation with 3% formaldehyde (FA). PBS 0.1% Triton X-100 was added to the fixed cells for 10 min prior to blocking with 3% bovine serum albumin in PBS for 1 h. ApiAT5-3::HA was visualised using rat anti-HA (1:500) followed by addition of Alexa594 conjugated donkey anti-rat secondary antibody (1:2000). SAG1 visualised with mouse anti-SAG1 (1:1000) and Alexa488 conjugated donkey anti-rat secondary antibody (1:2000). DAPI, 5 µg/ml.

Plaque assay and amino acid complementation

For plaque assay analysis, 150 parasites were seeded on confluent HFF monolayers, grown in 24-well plates, and left undisturbed for 5 days, before fixing with chilled methanol and staining with 0.1% crystal violet. To assess growth in excess tyrosine, plaque assays were repeated either at normal tyrosine levels (400 µM L-tyrosine disodium salt; as per Gibco manufacturer) or in DMEM supplemented with 2 mM L-tyrosine disodium salt (dissolved for 1 h at 50°C). To ensure tyrosine had successfully dissolved samples of the media were analysed by GC-MS as previously described (MacRae *et al.*, 2012).

Replication assay

2×10^4 ApiAT5-3_loxP parasites were seeded in triplicate on confluent HFFs in both culture flasks and glass

bottom 8-well imaging plates and left to invade for 1 h prior to treatment with 50 nM RAP or equivalent volume DMSO, for 4 h. Parasites were imaged at 24, 36 and/or 48 h and split at 36 h into new flasks and imaging wells for the subsequent replication cycle. At each time point parasites were fixed in 3% FA and imaged on a Nikon Eclipse Ti-U inverted fluorescent microscope. Parasites/vacuole were counted manually from five fields of view at 20× magnification using the Nikon NIS-Elements software.

Live cell microscopy

ApiAT5-3_loxP parasites were treated with RAP or DMSO as previously described. Thirty-six hours into cycle 2 post-RAP treatment parasites were syringe lysed and seeded in glass bottom, 8-well imaging plates in a 1:1 ratio with RH Tom parasites. After a further 29 h, live parasites were imaged on a Nikon Eclipse Ti-U inverted fluorescent microscope every 30 min for the next 30 h, in a temperature-controlled chamber at 37°C and 5% CO₂. Images were analysed using the Nikon NIS-Elements software.

Ionophore-induced egress assays

ApiAT5-3_loxP parasites were seeded in 96-well imaging plates at a MOI of 0.5, 36 h post-RAP/DMSO treatment. IIE assays were performed in triplicate at 37°C in Ringers buffer (155 mM NaCl, 3 mM KCl, 2 mM CaCl₂, 1 mM MgCl₂, 3 mM NaH₂PO₄, 10 mM HEPES, 10 mM glucose) 30 h later. The parasites were incubated with 8 µM Ca²⁺ ionophore A23187 for 0, 0.5, 1, 1.5, 2, 2.5, 3, 3.5, 4 and 5 min prior to the addition of 16% FA to a final concentration of 3% for 15 min. Wells were subsequently washed with PBS and stained with 5 µg/ml DAPI. Automated image acquisition of 25 fields per well was performed on a Cellomics Array Scan VTI HCS reader (Thermo Scientific) using a 20× objective. Image analysis was performed using the Compartmental Analysis BioApplication on HCS Studio (Thermo Scientific).

Competition assays and flow cytometry

For expression analysis of complemented lines, syringe lysed ApiAT5-3_loxP, $\Delta apiAT5-3^{ApiAT5-3}$, $\Delta apiAT5-3^{ApiAT5-3_{S56A}}$ and $\Delta apiAT5-3^{ApiAT5-3_{S56D}}$ lines were spun at 72 × g to remove host cell debris for 1 min. The supernatant was spun at 2049 × g for 5 min and the pellet fixed for 10 min in 3% FA. Fixed parasites were washed in PBS and resuspended in 0.1% Triton X-100 for 5 min prior to staining with anti-HA conjugated to allophycocyanin (1:500) for 1 h. The sample was washed and resuspended in PBS before running on a flow cytometer. For competition assays, 5×10^6 ApiAT5-3^{ApiAT5-3}, ApiAT5-3^{ApiAT5-3_{S56A}} and ApiAT5-3^{ApiAT5-3_{S56D}} parasites were mixed in a 1:1 ratio with $\Delta apiAT5-3^{ApiAT5-3}$, $\Delta apiAT5-3^{ApiAT5-3_{S56A}}$ and $\Delta apiAT5-3^{ApiAT5-3_{S56D}}$ respectively. 5×10^4 parasites

were added to fresh HFF monolayers prior to washing and fixation, as described previously. After fixation, parasites were stained with 5 µg/ml DAPI for 10 min and washed and resuspended in PBS before running on a flow cytometer. All parasites were gated on DAPI fluorescence to prevent results being skewed by remaining unstained host cell debris. The proportion of DAPI (+); YFP (+) (representing $\Delta\text{apiAT5-3}^{\text{ApiAT5-3/S56A/S56D}}$) compared to DAPI (+); YFP (-) (representing $\text{ApiAT5-3}^{\text{ApiAT5-3/S56A/S56D}}$) was calculated. The process was repeated 14 days later for comparison to day 0.

Oocyte maintenance and radiotracer uptake assays

ApiAT5-3 , $\text{ApiAT5-3}_{\text{S56A}}$ and $\text{ApiAT5-3}_{\text{S56D}}$ were PCR amplified from $\Delta\text{apiAT5-3}^{\text{ApiAT5-3}}$, $\Delta\text{apiAT5-3}^{\text{ApiAT5-3}_{\text{S56A}}}$ and $\Delta\text{apiAT5-3}^{\text{ApiAT5-3}_{\text{S56D}}}$ cDNA, respectively, using primers 29 and 30 to add a region of homology to the XkbN plasmid at the 5' end and a HA tag to the 3' end of each gene. These fragments were then amplified with primers 31 and 32 to add a 3' XkbN homology overhang. These resulting fragments were inserted by Gibson assembly into the XkbN1_PfHT (a version of pSPGT1 (Woodrow *et al.*, 1999) with a NotI site added to the MCS, provided by Ksenija Slavic) which had been digested with BglIII and NotI, to remove the PfHT gene. The resulting XkbN_ApiAT5-3, XkbN_ApiAT5-3_S56A and XkbN_ApiAT5-3_S56D plasmids were linearised with XbaI for in vitro transcription using the Thermo Fisher mMessage mMachine transcription kit. Stage V to VI defolliculated *X. laevis* oocytes were obtained commercially (Ecocyte Biosciences) for subsequent functional transport studies. Oocytes were microinjected with cRNA (20 to 40 ng in 30 nl of water) encoding *apiAT5-3* template or with a comparable amount of diethylpyrocarbonate-treated water. The oocytes were maintained at 18°C in oocyte Ringer 2 buffer (82.5 mM NaCl, 2.5 mM KCl, 1.5 mM CaCl₂, 1 mM Na₂HPO₄, 1 mM MgCl₂ and 5 mM HEPES) and used for transport studies 72 h after cRNA injection. Transport measurements were performed at room temperature on groups of 10 oocytes in ND96 medium (96 mM NaCl, 2 mM KCl, 2 mM CaCl₂, 1 mM MgCl₂ and 5 mM HEPES) containing 1 µM radiolabelled U-¹⁴C-L-tyrosine (specific activity of 486 mCi/mmol; Perkin Elmer), U-¹⁴C-L-phenylalanine (specific activity of 508 mCi/mmol; Perkin Elmer) or U-¹⁴C-L-valine (specific activity of 271 mCi/mmol; Perkin Elmer). Transport was measured at 10 min, over which time uptake of L-tyrosine is linear (Parker *et al.*, 2018). Each result was confirmed by at least three independent experiments.

Metabolite labelling and extraction

$\text{ApiAT5-3}_{\text{loxP}}$, $\Delta\text{apiAT5-3}^{\text{ApiAT5-3}}$, $\Delta\text{apiAT5-3}^{\text{ApiAT5-3}_{\text{S56A}}}$ and $\Delta\text{apiAT5-3}^{\text{ApiAT5-3}_{\text{S56D}}}$ parasites were treated in triplicate with 50 nM RAP and, at the end of the first cycle, seeded in 15 cm culture flasks. Stable isotope

labelling (1 h) of extracellular parasites with 0.8 mM U-¹³C-L-tyrosine or 4 mM U-¹³C-L-isoleucine, metabolite extraction and subsequent GC-MS analysis were all performed as per (MacRae *et al.*, 2012), on an Agilent GC-MSD (7890B-5977A). Data analysis was carried out using GAVIN software (Behrends *et al.*, 2011).

RNA sequencing analysis

T. gondii RNA was extracted as per the Qiagen RNeasy mini kit user handbook (#74104) from $\sim 5 \times 10^6$ $\text{ApiAT5-3}_{\text{loxP}}$ or $\text{ApiAT5-3}_{\text{loxP}}^{\text{dDiCre}}$ parasites at 0, 4 and 60 h post-RAP treatment. Analysis was performed in triplicate. The FASTQ files were aligned using Bowtie 2 (Langmead and Salzberg, 2012) to Ensembl Protist release 35 of *T. gondii* (ToxoDB-7.1). They were then quantified using RSEM before being processed using Bioconductor (Huber *et al.*, 2015). We used DESeq2 (Love *et al.*, 2014) to account for gene length and library size, and to test for the interaction between treatment and time point to generate the differential genelist. We corrected for multiple testing using the Benjamini–Hochberg procedure for false discovery rates. To validate the recodonised transcript, we both re-aligned to a custom genome rebuilt to include the novel sequence, and also used a pseudo-alignment approach to quantify purely the reads associated with the novel sequence (Bray *et al.*, 2016).

Acknowledgements

We thank all members of the Treeck laboratory for critical discussions. We thank Giel Van Dooren and Sebastian Lourido for sharing unpublished data. We thank members of the following Science Technology platforms at the Francis Crick Institute: Bioinformatics, Advanced Sequencing, Peptide Synthesis, Proteomics and Flow Cytometry. This work was supported by awards to MT by the National Institute of Health (NIH-R01A123457) and The Francis Crick Institute (<https://www.crick.ac.uk/>), which receives its core funding from Cancer Research UK (FC001189; <https://www.cancerresearchuk.org/>), the UK Medical Research Council (FC001189; <https://www.mrc.ac.uk/>) and the Wellcome Trust (FC001189; <https://wellcome.ac.uk/>). HMS is supported by the Wellcome Trust Institutional Strategic Support Fund (204809/Z/16/Z) awarded to St. George's University of London.

Conflicts of interest

The authors confirm that there are no conflicts of interest with the contents of this article.

Author contributions

BAW and MT conceived experiments and wrote the paper. BAW, CSD and MB designed and performed

experiments and data analysis. NL performed experiments and data analysis. JIM and HMS helped conceive experiments and edited the paper.

References

- Abramian, A.M., Comenencia-Ortiz, E., Modgil, A., Vien, T.N., Nakamura, Y., Moore, Y.E., *et al.* (2014) Neurosteroids promote phosphorylation and membrane insertion of extrasynaptic GABAA receptors. *Proceedings of the National Academy of Sciences*, **111**, 7132–7137.
- Andenmatten, N., Egarter, S., Jackson, A.J., Jullien, N., Herman, J.-P. and Meissner, M. (2013) Conditional genome engineering in *Toxoplasma gondii* uncovers alternative invasion mechanisms. *Nature Methods*, **10**, 125–127.
- Aryal, B., Laurent, C. and Geisler, M. (2015) Learning from each other: ABC transporter regulation by protein phosphorylation in plant and mammalian systems. *Biochemical Society Transactions*, **43**, 966–974.
- Babbitt, S.E., Altenhofen, L., Cobbold, S.A., Istvan, E.S., Fennell, C., Doerig, C., *et al.* (2012) Plasmodium falciparum responds to amino acid starvation by entering into a hibernatory state. *Proceedings of the National Academy of Sciences*, **109**, E3278–E3287.
- Behrends, V., Tredwell, G.D. and Bundy, J.G. (2011) A software complement to AMDIS for processing GC-MS metabolomic data. *Analytical Biochemistry*, **415**, 206–208.
- Billker, O., Lourido, S. and Sibley, L.D. (2009) Calcium-dependent signaling and kinases in Apicomplexan parasites. *Cell Host & Microbe*, **5**, 612–622.
- Black, M.W., Arrizabalaga, G. and Boothroyd, J.C. (2000) Ionophore-resistant mutants of *Toxoplasma gondii* reveal host cell permeabilization as an early event in egress. *Molecular and Cellular Biology*, **20**, 9399–9408.
- Bray, N.L., Pimentel, H., Melsted, P. and Pachter, L. (2016) Near-optimal probabilistic RNA-seq quantification. *Nature Biotechnology*, **34**, 525–527.
- Carruthers, V.B. and Sibley, L.D. (1999) Mobilization of intracellular calcium stimulates microneme discharge in *Toxoplasma gondii*. *Molecular Microbiology*, **31**, 421–428.
- Endo, T., Sethi, K.K. and Piekarski, G. (1982) *Toxoplasma gondii*: calcium ionophore A23187-mediated exit of trophozoites from infected murine macrophages. *Experimental Parasitology*, **53**, 179–188.
- Gaji, R.Y., Johnson, D.E., Treeck, M., Wang, M., Hudmon, A. and Arrizabalaga, G. (2015) Phosphorylation of a myosin motor by TgCDPK3 facilitates rapid initiation of motility during *Toxoplasma gondii* egress. *PLoS Pathogens*, **11**, e1005268.
- Garrison, E., Treeck, M., Ehret, E., Butz, H., Garbuz, T., Oswald, B.P., *et al.* (2012) A forward genetic screen reveals that calcium-dependent protein kinase 3 regulates egress in *Toxoplasma*. *PLoS Pathogens*, **8**, e1003049.
- Gibson, D.G., Benders, G.A., Andrews-Pfannkoch, C., Denisova, E.A., Baden-Tillson, H., Zaveri, J., *et al.* (2008) Complete chemical synthesis, assembly, and cloning of a *Mycoplasma genitalium* genome. *Science*, **319**, 1215–1220.
- Hofmann, K. (1993) TMbase – A database of membrane spanning proteins segments. *Biological Chemistry Hoppe-Seyler*, **374**, 166.
- Huang, J.F., Teyton, L. and Harper, J.F. (1996) Activation of a Ca²⁺-dependent protein kinase involves intramolecular binding of a calmodulin-like regulatory domain. *Biochemistry*, **35**, 13222–13230.
- Huber, W., Carey, V.J., Gentleman, R., Anders, S., Carlson, M., Carvalho, B.S., *et al.* (2015) Orchestrating high-throughput genomic analysis with Bioconductor. *Nature Methods*, **12**, 115–121.
- Jang, H.-Y., Rhee, J., Carlson, J.E. and Ahn, S.-J. (2014) The Camelina aquaporin CsPIP2;1 is regulated by phosphorylation at Ser273, but not at Ser277, of the C-terminus and is involved in salt- and drought-stress responses. *Journal of Plant Physiology*, **171**, 1401–1412.
- Langmead, B. and Salzberg, S.L. (2012) Fast gapped-read alignment with Bowtie 2. *Nature Methods*, **9**, 357–359.
- Lee, S.C., Lan, W.-Z., Kim, B.-G., Li, L., Cheong, Y.H., Pandey, G.K., *et al.* (2007) A protein phosphorylation/dephosphorylation network regulates a plant potassium channel. *Proceedings of the National Academy of Sciences*, **104**, 15959–15964.
- Liu, K.-H. and Tsay, Y.-F. (2003) Switching between the two action modes of the dual-affinity nitrate transporter CHL1 by phosphorylation. *The EMBO Journal*, **22**, 1005–1013.
- Long, S., Wang, Q. and Sibley, L.D. (2016) Analysis of non-canonical calcium dependent protein kinases in *Toxoplasma gondii* by targeted gene deletion using CRISPR/Cas9. *Infection and Immunity*, **84**(5), 1262–1273.
- Lourido, S. and Moreno, S.N. (2015) The calcium signaling toolkit of the Apicomplexan parasites *Toxoplasma gondii* and Plasmodium spp. *Cell Calcium*, **57**, 186–193.
- Lourido, S., Tang, K. and Sibley, L.D. (2012) Distinct signalling pathways control *Toxoplasma* egress and host-cell invasion. *The EMBO Journal*, **31**, 4524–4534.
- Lourido, S., Jeschke, G.R., Turk, B.E. and Sibley, L.D. (2013) Exploiting the unique ATP-binding pocket of *Toxoplasma* calcium-dependent protein kinase 1 to identify its substrates. *ACS Chemical Biology*, **8**, 1155–1162.
- Love, M.I., Huber, W. and Anders, S. (2014) Moderated estimation of fold change and dispersion for RNA-seq data with DESeq2. *Genome Biology*, **15**, 1–21.
- Lovett, J.L. and Sibley, L.D. (2003) Intracellular calcium stores in *Toxoplasma gondii* govern invasion of host cells. *Journal of Cell Science*, **116**, 3009–3016.
- MacRae, J.I., Sheiner, L., Nahid, A., Tonkin, C., Striepen, B. and McConville, M.J. (2012) Mitochondrial metabolism of glucose and glutamine is required for intracellular growth of *Toxoplasma gondii*. *Cell Host & Microbe*, **12**, 682–692.

- Marino, N.D. and Boothroyd, J.C. (2017) *Toxoplasma* growth in vitro is dependent on exogenous tyrosine and is independent of AAH2 even in tyrosine-limiting conditions. *Experimental Parasitology*, **176**, 52–58.
- McCoy, J.M., Whitehead, L., van Dooren, G.G. and Tonkin, C.J. (2012) TgCDPK3 regulates calcium-dependent egress of *Toxoplasma gondii* from host cells. *PLoS Pathogens*, **8**, e1003066.
- Mondragon, R. and Frixione, E. (1996) Ca²⁺-dependence of conoid extrusion in *Toxoplasma gondii* tachyzoites. *The Journal of Eukaryotic Microbiology*, **43**, 120–127.
- Moudy, R., Manning, T.J. and Beckers, C.J. (2001) The loss of cytoplasmic potassium upon host cell breakdown triggers egress of *Toxoplasma gondii*. *Journal of Biological Chemistry*, **276**, 41492–41501.
- Nebi, T., Prieto, J.H., Kapp, E., Smith, B.J., Williams, M.J., Yates, J.R. 3rd, et al. (2011) Quantitative in vivo analyses reveal calcium-dependent phosphorylation sites and identifies a novel component of the *Toxoplasma* invasion motor complex. *PLoS Pathogens*, **7**, e1002222.
- Nissen-Meyer, L.S.H., Popescu, M.C., Hamdani, E.H. and Chaudhry, F.A. (2011) Protein kinase C-mediated phosphorylation of a single serine residue on the rat glial glutamine transporter SN1 governs its membrane trafficking. *Journal of Neuroscience*, **31**, 6565–6575.
- Oppenheim, R.D., Creek, D.J., Macrae, J.I., Modrzynska, K.K., Pino, P., Limenitakis, J., et al. (2014) BCKDH: the missing link in apicomplexan mitochondrial metabolism is required for full virulence of *Toxoplasma gondii* and *Plasmodium berghei*. *PLoS Pathogens*, **10**, e1004263.
- Parker, K.E.R., Fairweather, S.J., Rajendran, E., Blume, M., McConville, M.J., Broer, S., et al. (2018) Characterization of the apicomplexan amino acid transporter (ApiAT) family in *Toxoplasma gondii*. *BioRxiv* 306993. Epub ahead of Print Available at: <https://www.biorxiv.org/content/early/2018/04/26/306993>.
- Ramamoorthy, S., Shippenberg, T.S. and Jayanthi, L.D. (2010) Regulation of monoamine transporters: role of transporter phosphorylation. *Pharmacology & Therapeutics*, **129**, 220–238.
- Rice, W.L., Zhang, Y., Chen, Y., Matsuzaki, T., Brown, D. and Lu, H.A.J. (2012) Differential, phosphorylation dependent trafficking of AQP2 in LLC-PK1 cells. *PLoS ONE*, **7**, e32843.
- Saeij, J.P.J., Boyle, J.P., Collier, S., Taylor, S., Sibley, L.D., Brooke-Powell, E.T., et al. (2006) Polymorphic secreted kinases are key virulence factors in Toxoplasmosis. *Science*, **314**, 1780–1783.
- Shen, B., Brown, K.M., Lee, T.D. and Sibley, L.D. (2014) Efficient gene disruption in diverse strains of *Toxoplasma gondii* using CRISPR/CAS9. *mBio*, **5**, e01114.
- Sidik, S.M., Hortua Triana, M.A., Paul, A.S., El Bakkouri, M., Hackett, C.G., Tran, F., et al. (2016) Using a genetically encoded sensor to identify inhibitors of *Toxoplasma gondii* Ca²⁺ signalling. *The Journal of Biological Chemistry*, **291**, 9566–9580.
- Sidik, S.M., Huet, D., Ganesan, S.M., Huynh, M.-H., Wang, T., Nasamu, A.S., et al. (2016) A genome-wide CRISPR screen in *Toxoplasma* identifies essential Apicomplexan genes. *Cell*, **166**, 1423–1435.
- Soldati, D. and Boothroyd, J.C. (1993) Transient transfection and expression in the obligate intracellular parasite *Toxoplasma gondii*. *Science*, **260**, 349–352.
- Stewart, R.J., Whitehead, L., Nijagal, B., Sleebs, B.E., Lessene, G., McConville, M.J., et al. (2016) Analysis of Ca²⁺ mediated signalling regulating *Toxoplasma* infectivity reveals complex relationships between key molecules. *Cellular Microbiology*, **19**, e12685.
- Tamura, N., Oku, M., Ito, M., Noda, N.N., Inagaki, F. and Sakai, Y. (2013) Atg18 phosphoregulation controls organellar dynamics by modulating its phosphoinositide-binding activity. *The Journal of Cell Biology*, **202**, 685–698.
- Thompson, A., Schäfer, J., Kuhn, K., Kienle, S., Schwarz, J., Schmidt, G., et al. (2003) Tandem mass tags: a novel quantification strategy for comparative analysis of complex protein mixtures by MS/MS. *Analytical Chemistry*, **75**, 1895–1904.
- Treeck, M., Sanders, J.L., Gaji, R.Y., LaFavers, K.A., Child, M.A., Arrizabalaga, G., et al. (2014) The calcium-dependent protein kinase 3 of *Toxoplasma* influences basal calcium levels and functions beyond egress as revealed by quantitative phosphoproteome analysis. *PLoS Pathogens*, **10**, e1004197.
- Wang, Z.T., Verma, S.K., Dubey, J.P. and Sibley, L.D. (2017) The aromatic amino acid hydroxylase genes AAH1 and AAH2 in *Toxoplasma gondii* contribute to transmission in the cat. *PLOS Pathogens*, **13**, e1006272.
- Wernimont, A.K., Artz, J.D., Finerty, P. Jr, Lin, Y.H., Amani, M., Allali-Hassani, A., et al. (2010) Structures of apicomplexan calcium-dependent protein kinases reveal mechanism of activation by calcium. *Nature Structural & Molecular Biology*, **17**, 596–601.
- Wernimont, A.K., Amani, M., Qiu, W., Pizarro, J.C., Artz, J.D., Lin, Y.H., et al. (2011) Structures of parasitic CDPK domains point to a common mechanism of activation. *Proteins*, **79**, 803–820.
- Wetzel, D.M., Chen, L.A., Ruiz, F.A., Moreno, S.N. and Sibley, L.D. (2004) Calcium-mediated protein secretion potentiates motility in *Toxoplasma gondii*. *Journal of Cell Science*, **117**, 5739–5748.
- Woodrow, C.J., Penny, J.I. and Krishna, S. (1999) Intraerythrocytic *Plasmodium falciparum* expresses a high affinity facilitative hexose transporter. *Journal of Biological Chemistry*, **274**, 7272–7277.

Supporting Information

Additional supporting information may be found online in the Supporting Information section at the end of the article.